Technical report

Resistivity and Induced Polarization Survey

Philibert Project
Chapais Area, James Bay Region, Québec
2018

Mosaic Minerals Inc.
4908 Pine Crescent
Vancouver, BC, Canada
V6M 3P6

Dynamic
Discovery
Geoscience

Prepared by
Joël Dubé, P.Eng.

December 2018

Dynamic Discovery Geoscience
7977 Décarie Drive
Ottawa (Ontario) K1C 3K3
jdube@ddgeoscience.ca

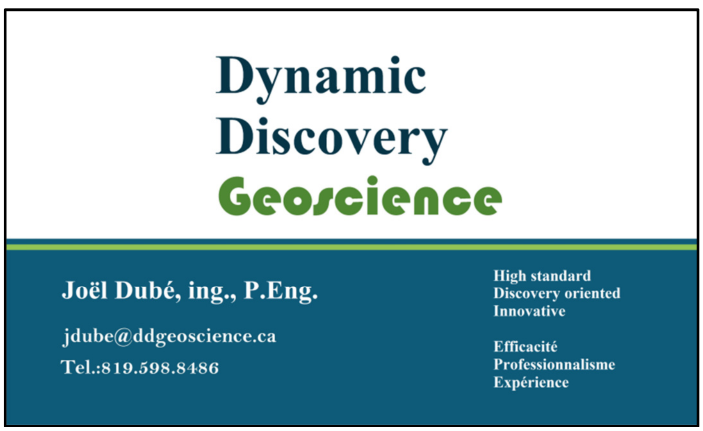

TABLE OF CONTENT

FIGURES

TABLES

I. INTRODUCTION

At the request of Mosaic Minerals Inc., a resistivity and induced polarization (IP) survey was performed on the Philibert Project, under the technical supervision of Dynamic Discovery Geoscience Ltd. The survey was conducted from November 4th to 11th, 2018, for a total production of 20.275 linear km.

The goal of the survey was to characterize the sub-surface rocks with respect to their signature to IP method, and to identify responses possibly associated to sulphides mineralized occurrences. The survey also aimed at understanding the geophysical characteristics of the "Philibert - Indice 1" gold occurrence found within the Philibert Property, and at identifying possible extensions to known mineralization. In order to provide assistance in the data interpretation process, airborne magnetic data owned by Mosaic Minerals are also used.

Figure 1: General location of the Philibert Project

II. PHILIBERT PROJECT

The Philibert Project consists of a block of 4 mineral claims located about 45 km to the southeast of the village of Chapais, within NTS map sheet 032G07 (Figure 2), and is accessed via forestry roads connecting to highway 113.

Figure 2: Regional location of the Philibert Project

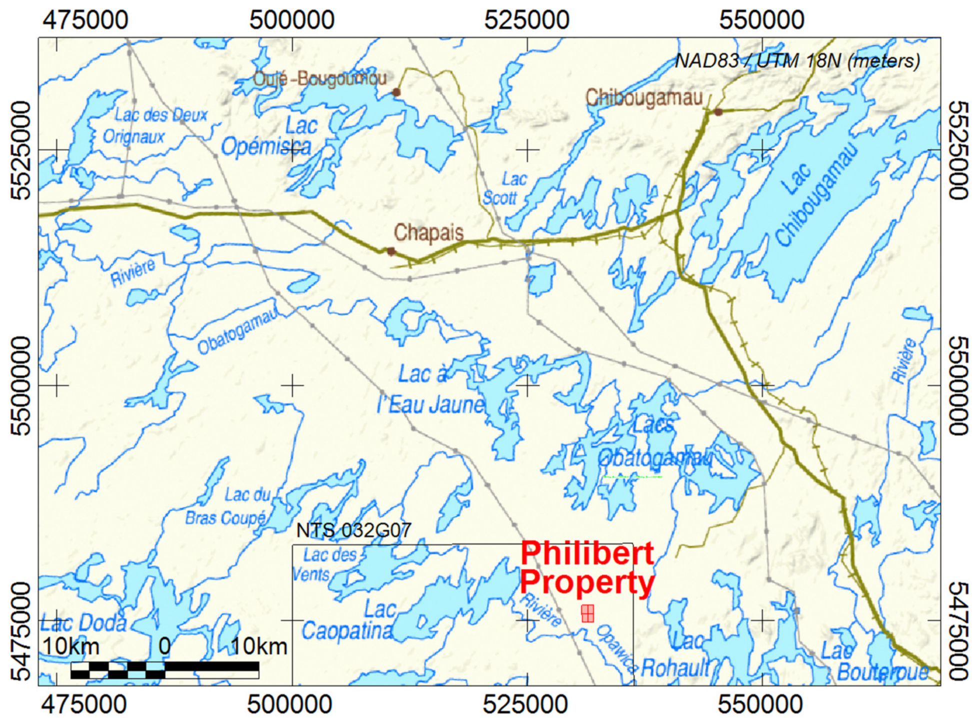

A survey grid has been prepared over the area. It consists of a network of 11 lines (L0E to L1000E) of 1.85 km in length, oriented N000 and spaced every 100 m (Figure 3). One baseline and two tie-lines, each 1 km long, were also cut perpendicular to survey lines, but were not surveyed, for a grand total of 23.35 km of line cutting. Lines were cut and chained by a team under the supervision of Mr. Samuel Choquette. A handheld GPS unit was used by the line cutters to record survey stations locations every 500 m or so along survey lines with an absolute accuracy of 2 to 5 m. This grid has been the subject of the IP survey. The active mineral claim titles covered by the survey are shown in red on Figure 3, and are listed in Table 1.

Table 1: Mineral claims covered by the survey

Mineral Claim
2235885
2235886

Mineral Claim
2238231
2238232

Figure 3: Digital elevation model with surveyed lines and active mineral claims

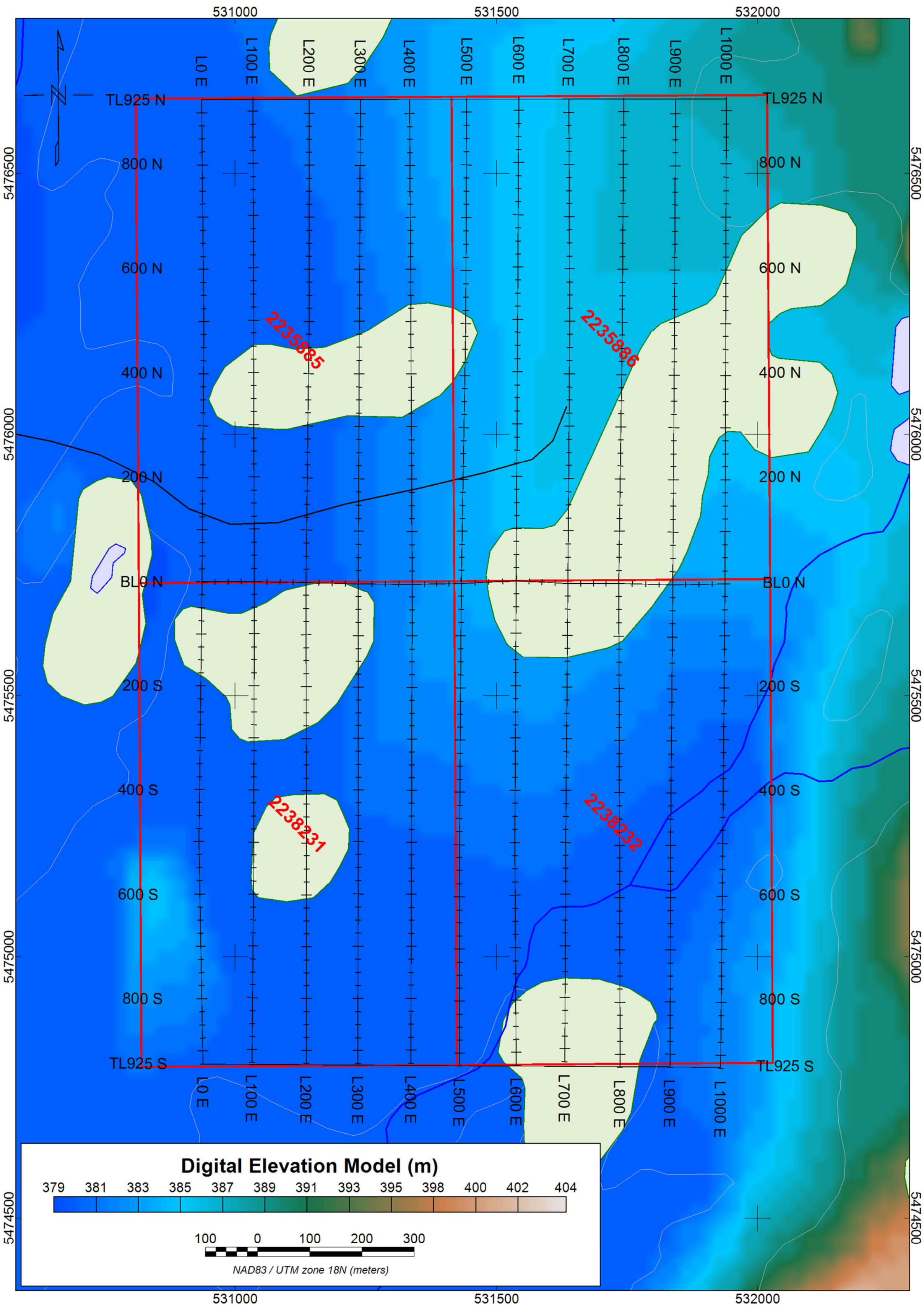

III. GEOPHYSICAL SURVEY TECHNICAL SPECIFICATIONS

Field Operations

The IP survey, totalling 20.275 km, was performed by one survey crew of Géophysique TMC from Val-d'Or, which was managed by Mr. Paul Mélançon. The IP survey took place from November 4th to 11th 2018. A total of 4542 data samples were recorded.

Technical supervision was provided by Mr. Joël Dubé, P.Eng., of Dynamic Discovery Geoscience in Ottawa. On top of data inspection performed on the field by the operator while conducting the survey and after transferring the data to a computer, the data was sent to Dynamic Discovery Geoscience's office on a daily basis to undergo full data QC. All data were verified in this manner before authorizing demobilization of the survey crew from the field.

IP Survey Equipment

The equipment used for the IP survey was made of a transmitting and a receiving circuit operating in time domain. An Instrumentation GDD TXII transmitter, with a power of 1800 W, was used to create the current square wave form. The source of current was supplied by a 2.5 kW motor generator. Stainless steel electrodes were used to ensure measurements' stability. The transmitter signal had an effective half-cycle of 2 seconds (Figure 4).

Figure 4: Signal generated by the transmitter

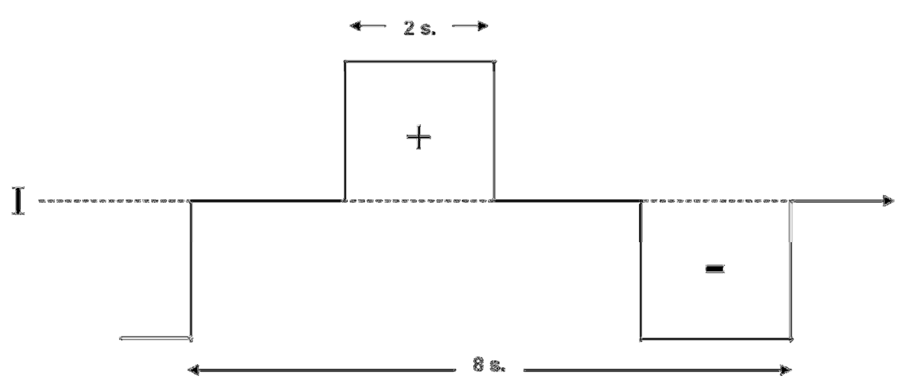

The primary voltage V_P and the chargeability M were recorded by an Elrec-Pro receiver from IRIS Instruments. Integration of the transient voltage after current shut-off was achieved using 20 time windows of equal duration, as shown in Figure 5. During survey acquisition on the field, the chargeability recorded for each window was normalized to Newmont standards, which enabled identification of electromagnetic coupling effects, of abnormally strong telluric noise or of any other type of interference requiring to be addressed before continuing the survey. A minimum of 8 half-cycles were recorded at each measurement point.

Figure 5: Windows used for signal integration at the receiver

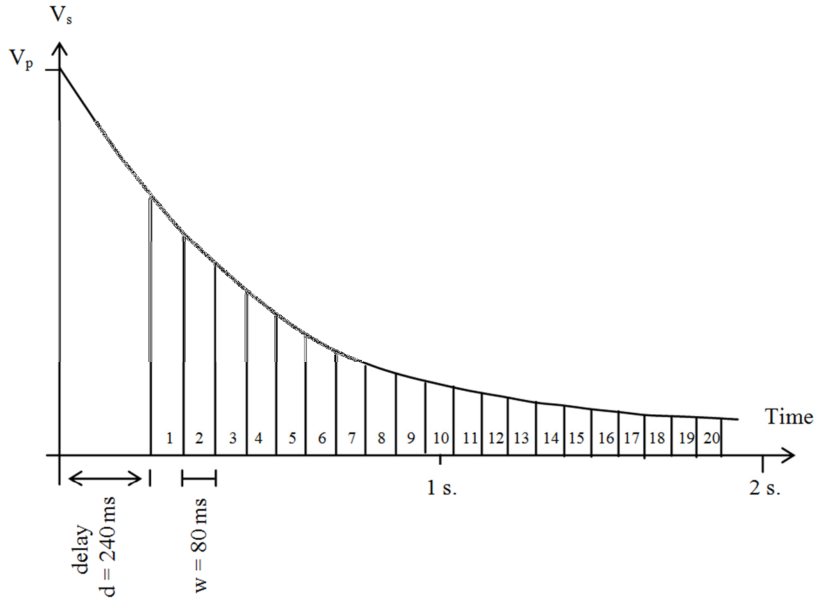

Electrode Array Configuration

The dipole-dipole array was used for this survey. This electrode configuration, shown in Figure 6, enables an easier anomaly detection and interpretation given the increased contrast of anomalies with respect to the background and the response symmetry that it provides. However, it decreases the signal to noise ratio and depth of investigation compared to the pole-dipole array. The number of measured dipoles (n) was set to 6. The electrode spacing (a) was set to 25 meters. This enables high spatial resolution, yet achieving a decent penetration depth of approximately 55 meters, which is sufficient given that the overburden thickness is limited in the area.

Figure 6: Dipole-dipole array configuration

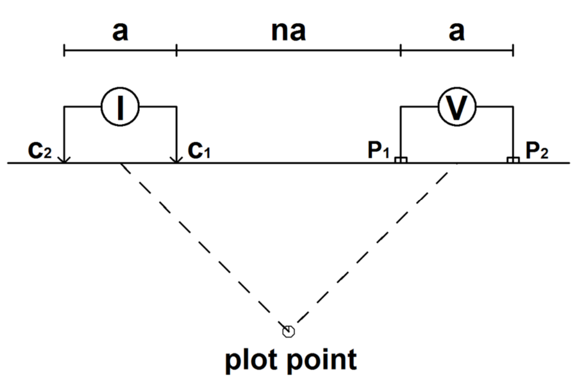

Apparent Resistivity and Chargeability Calculation

Apparent chargeability (*Ma*) is obtained by calculation of the average of the normalized chargeability for each of the 20 linear time windows and is expressed in mV/V. When the decay curve diverts too much from a pure polarization effect and is clearly affected by noise, the chargeability value is discarded from the database and is not used. This usually occurs when the signal received at potential electrodes is simply too weak to yield a reliable measurement, due to the occurrence of a very strong conductor underneath the survey setup.

Apparent resistivity (ρ_a), expressed in Ohm-m, was calculated using the following equation :

$$\rho_a = K\, V_P / I \quad ; \quad K = 2\pi / [(1/r1)-(1/r2)-(1/r3)+(1/r4)]$$

where V_p = peak voltage (mV)
I = current applied to the ground (mA)
K = geometrical factor taking into account the location of each electrode used, with
r1 = distance between C_1 and P_1 (m)
r2 = distance between C_2 and P_1 (m)
r3 = distance between C_1 and P_2 (m)
r4 = distance between C_2 and P_2 (m)

Taking into account the dipole-dipole array geometry, this expression can be rewritten as:

$$\rho_a = \pi \cdot n \cdot (n+1) \cdot (n+2) \cdot a \cdot (V_P / I)$$

Resistivity and Chargeability Inversion Models

In order to generate a probable representation of the sources causing the observed responses, an inversion software, RES2DINV distributed by Geotomo, was used. Unconstrained inversions of resistivity and chargeability data were performed to create 2D models of the distribution of these physical properties underneath each surveyed line.

Since the equation used to calculate the raw apparent resistivity assumes a flat topographical surface, taking into account the actual topography when performing the inversion enables a representation of the causative sources that is free of any topographical effects. True depth inversion models are considered very useful when it comes to planning follow-up work such as stripping and drilling.

IV. RESULTS AND DISCUSSION

Data Presentation

Data compilation including editing and filtering, quality control (QC), and final data processing was performed by Joël Dubé, P.Eng. Processing was performed on high performance computers optimized for rapid processing tasks. Geosoft software Oasis Montaj version 9.3.3 was used.

For each of the lines surveyed with the IP technique, sections have been created showing apparent resistivity and chargeability pseudo-sections, true-depth inversion models of resistivity and chargeability, as well as an interpretation line. The interpretation consists in series of interpretation boxes. Boxes above the interpretation line enable classification of chargeability anomalies based on their intensity. Four anomaly classes are used: marginal, weak, moderate and strong. Boxes below this line are used to classify resistivity classes, mainly to highlight correlations between chargeability and resistivity anomalies, and are simply divided into two categories: resistive or conductive. Interpretation boxes are located in the vertical projection of the area where the source is thought closest to surface. Chargeability anomalies that can be recognized and followed over multiple lines enabled the definition of polarizable axes or of compact networks of axes. These chargeable axes were given ID numbers, and these numbers are shown on sections, above chargeability interpretation boxes. The sections are provided at the 1:2,500 scale in digital form as PDF, PNG and Geosoft MAP files.

Results are also shown on plan maps. First of all, results from IP inversion models have been extracted at several depths for each line, and then interpolated between the lines to create grids showing the lateral changes of the resistivity and chargeability distribution within the ground. Results were extracted at depths of 10, 25 and 45 meters (Figures 7 to 12). The data grids shown on these images were created with a 12.5 m grid cell size, appropriate for the survey stations spaced every 25 m. Finally, an interpretation map was made, which integrates interpretation elements based on the airborne magnetic data available in the area (Paul, 2014) and on the newly acquired IP data (Figures 16 to 19). Mineralized showings as well as drill holes reported in Québec's Ministère de l'Énergie et des Ressources Naturelles (MERN) files are also shown on this map.

The First Vertical Derivative (FVD) of the Total Magnetic Intensity (TMI) taken from the Philibert Property airborne survey is shown in the background of Figure 17 and of the interpretation map to enable direct comparison of the IP interpretation with the magnetic data. All the maps created are referenced with respect to the NAD-83 datum, UTM zone 18N projection. They are supplied at a 1:5,000 scale in PDF, PNG, GeoTiff and Geosoft MAP formats. Grids of the results are also supplied in Geosoft GRD and GeoTiff formats. Finally, interpretation elements found on the interpretation map are supplied in the Esri SHP and GeoTiff formats. Table 2 provides a list of all the maps delivered.

Figure 7: Resistivity inversion model extracted at depth of 10m

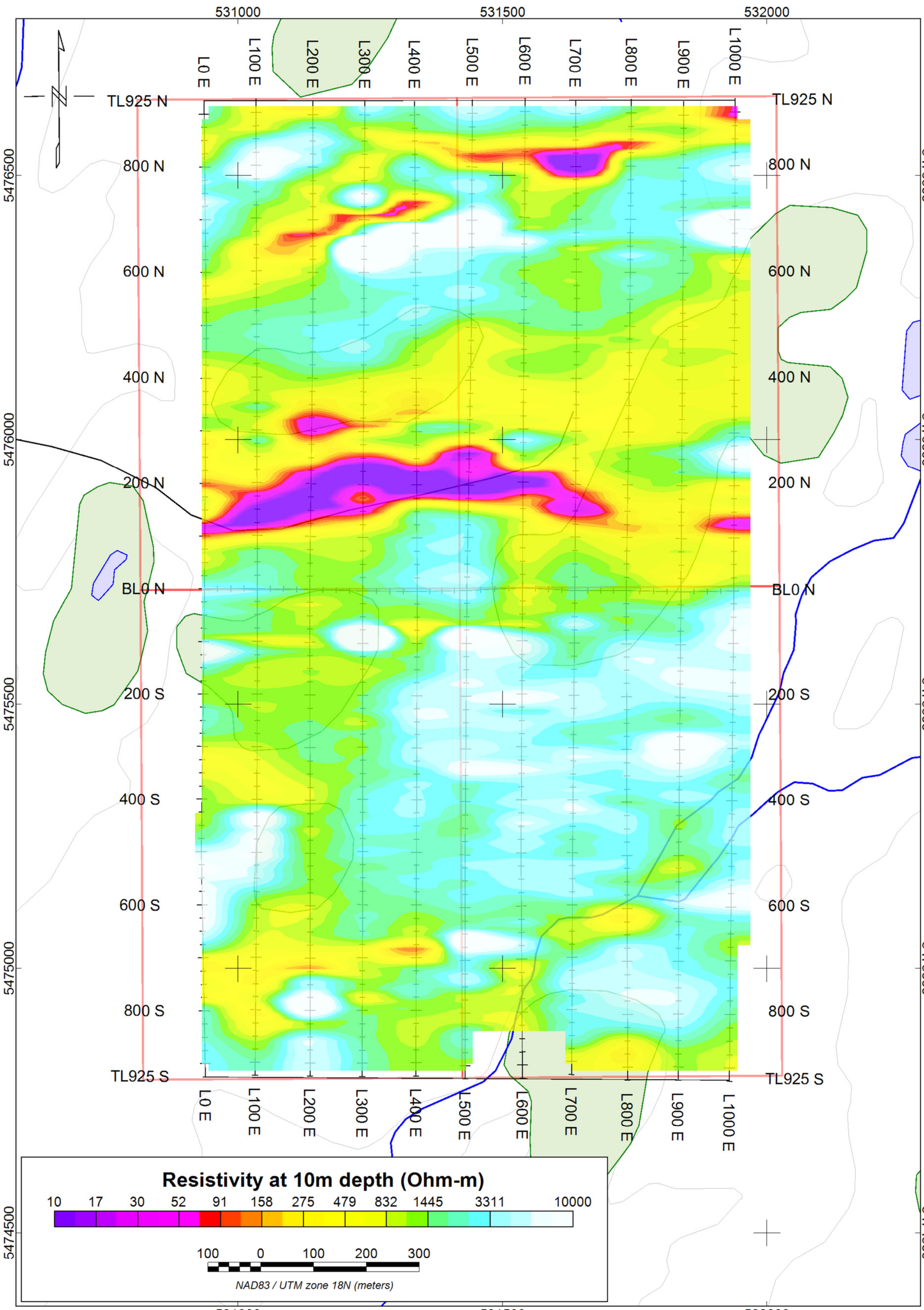

Figure 8: Resistivity inversion model extracted at depth of 25m

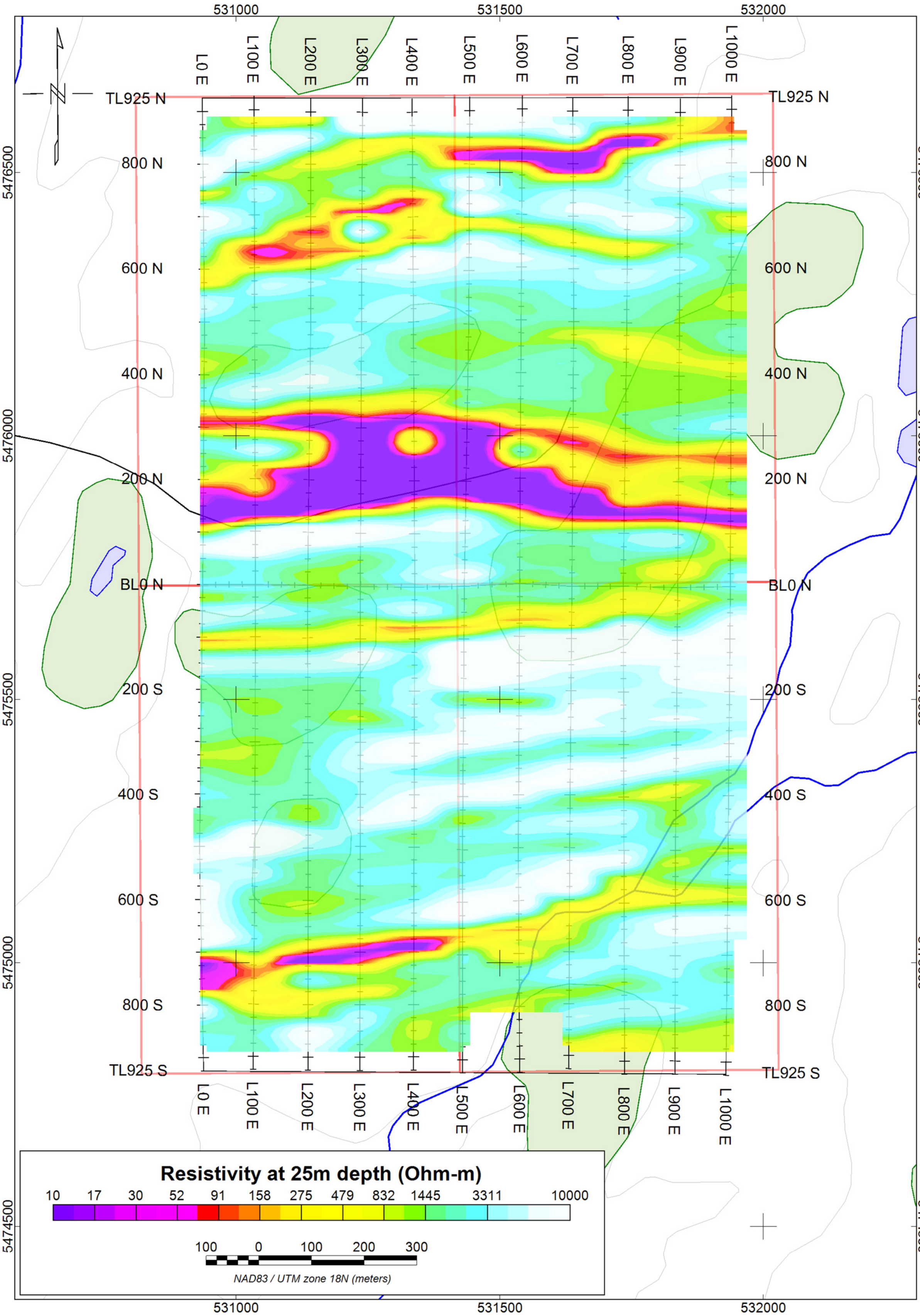

Figure 9: Resistivity inversion model extracted at depth of 45m

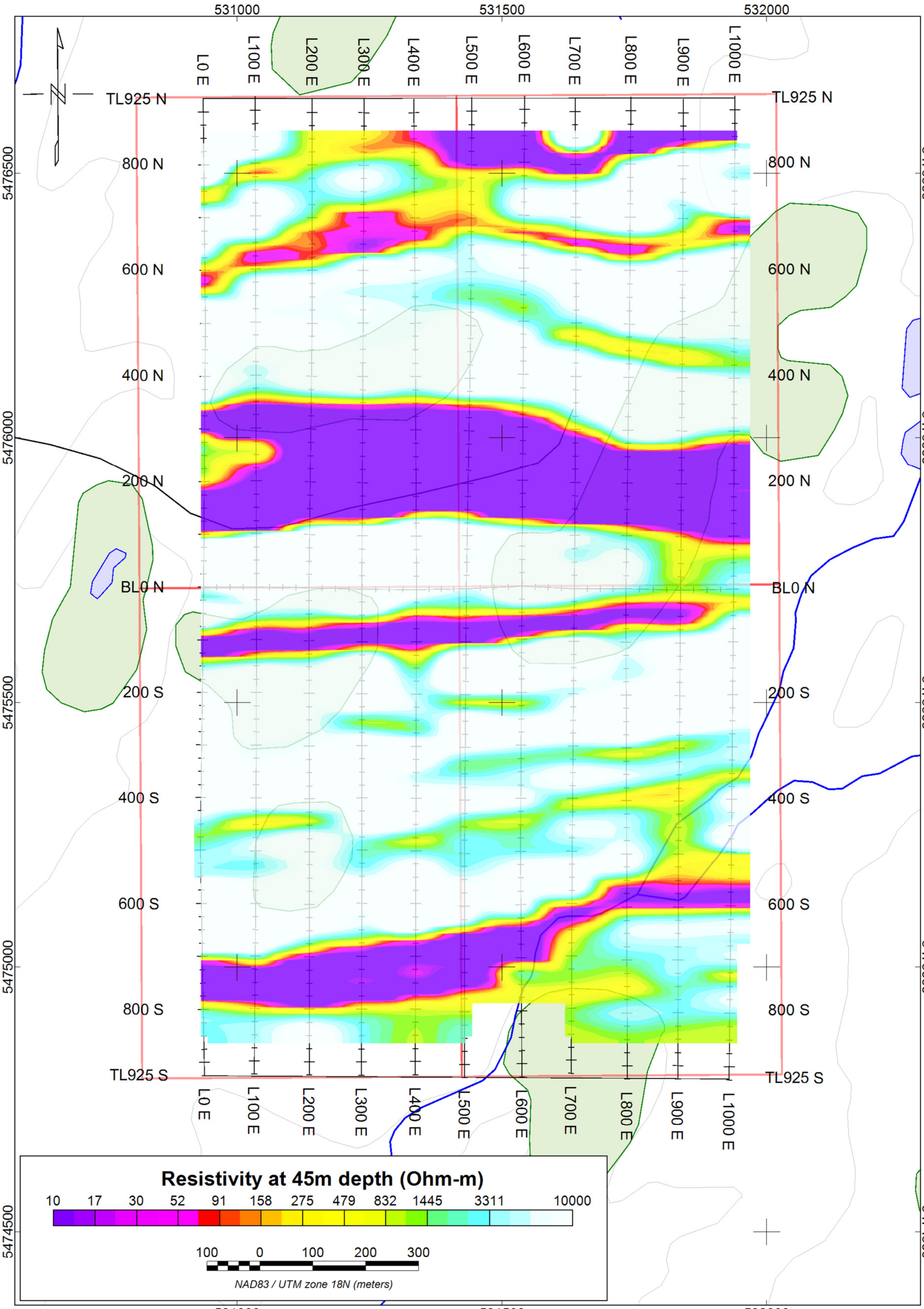

Figure 10: Chargeability inversion model extracted at depth of 10m

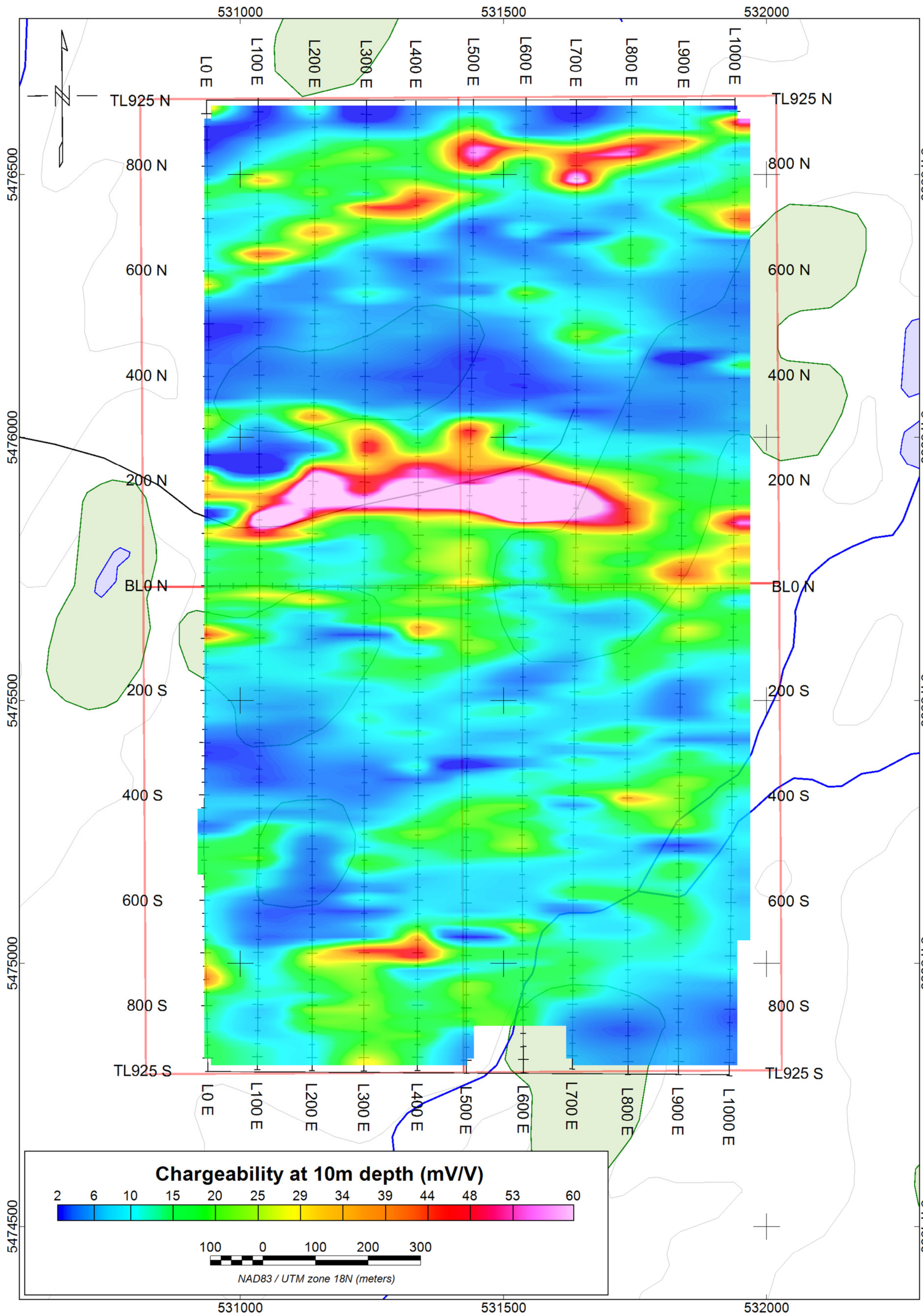

Figure 11: Chargeability inversion model extracted at depth of 25m

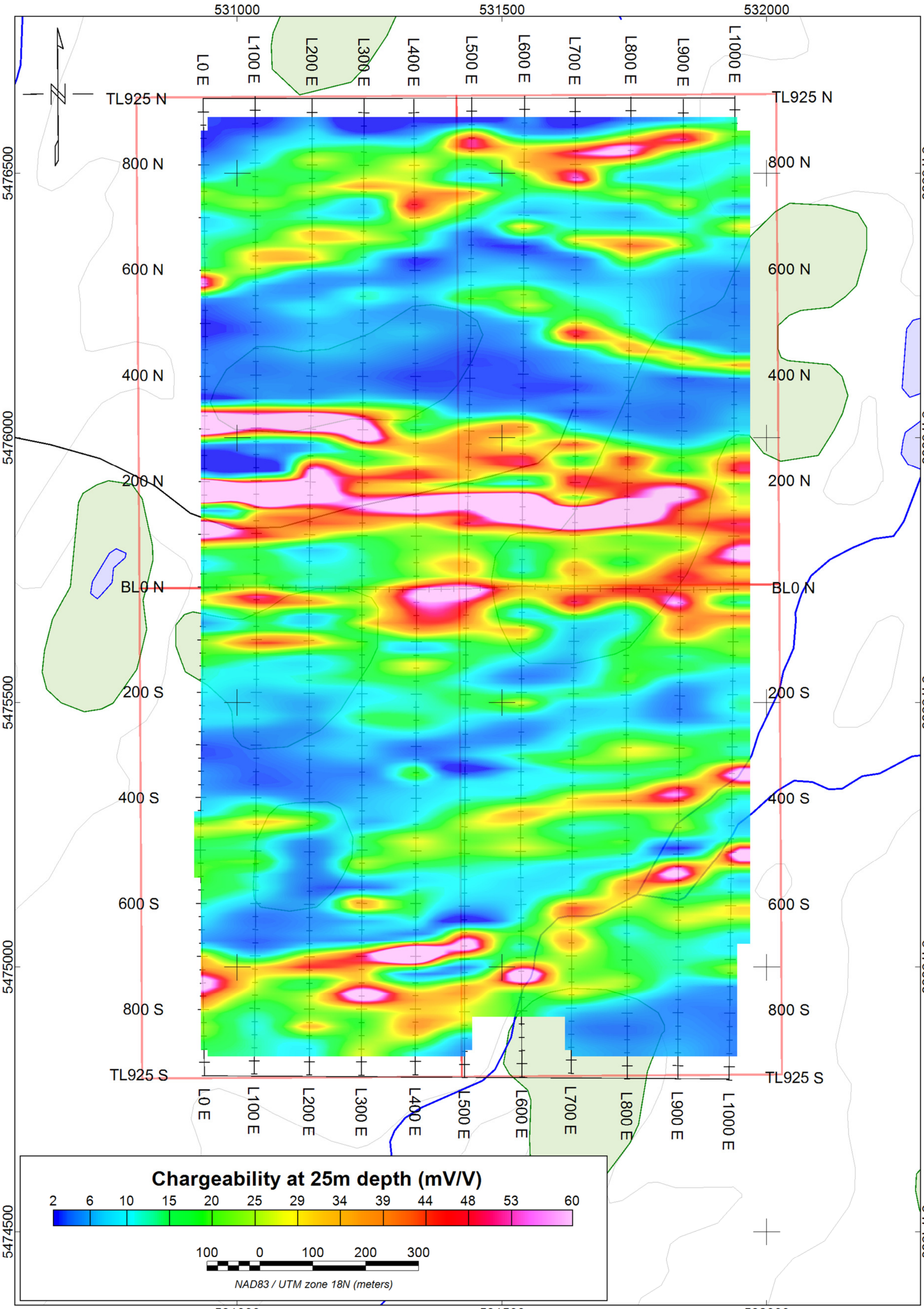

Figure 12: Chargeability inversion model extracted at depth of 45m

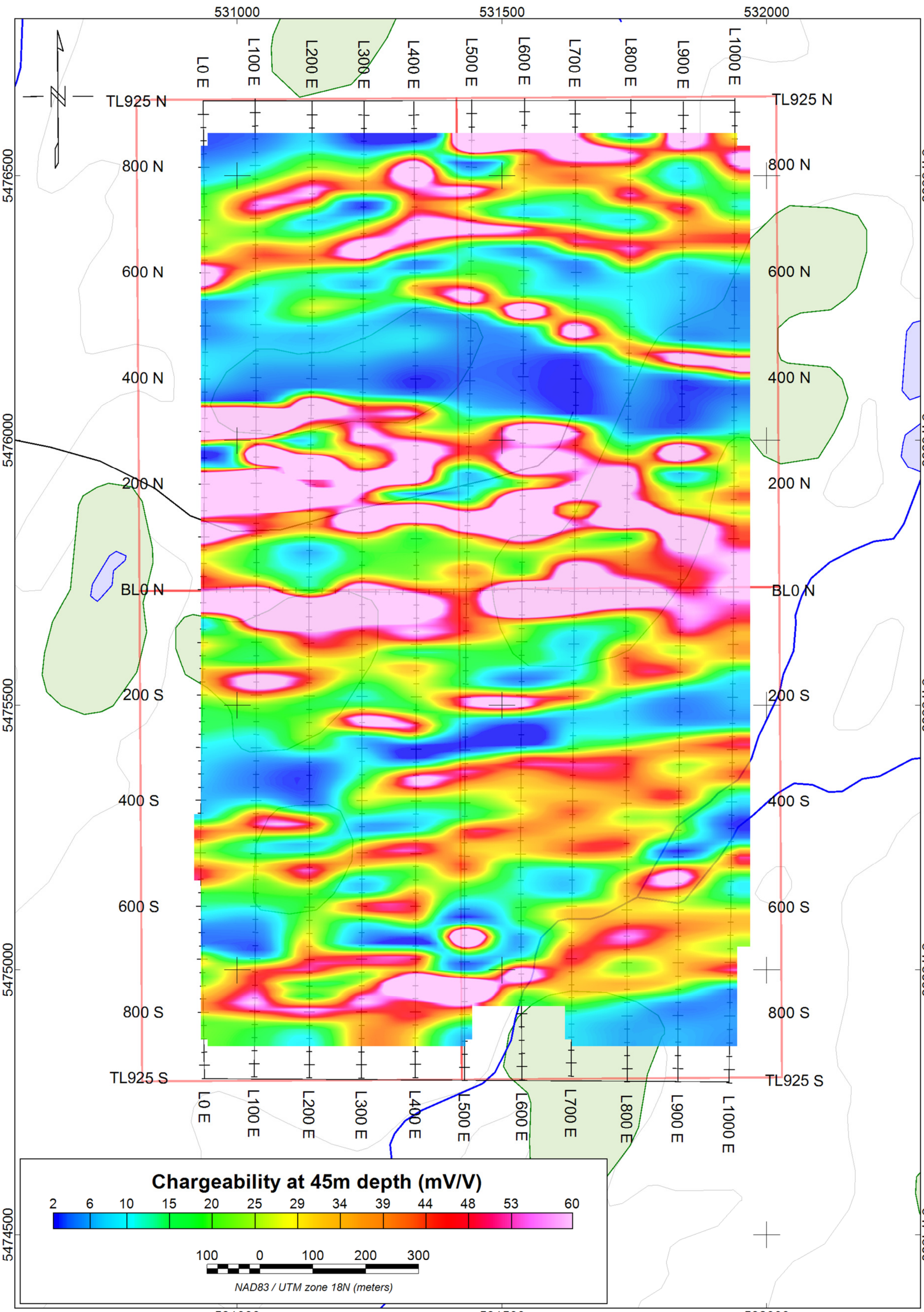

Table 2: List of maps

No.	Name	Description
1	DEM	Geographic location of survey lines and mining claims on top of DEM
2	RES10m	Resistivity inversion model extracted at a depth of 10m
3	RES25m	Resistivity inversion model extracted at a depth of 25m
4	RES45m	Resistivity inversion model extracted at a depth of 45m
5	CHA10m	Chargeability inversion model extracted at a depth of 10m
6	CHA25m	Chargeability inversion model extracted at a depth of 25m
7	CHA45m	Chargeability inversion model extracted at a depth of 45m
8	Interpretation	Interpretation of resistivity and IP survey on top of airborne magnetics

IP inversion models were also interpolated in 3D to create voxels (3D grids), enabling tridimensional visualisation of the physical properties distribution within the ground. Figure 13 shows the topography of the surveyed area, which is very flat, while Figures 14 and 15 show the resistivity and chargeability inversion models, all with a 45° plunging view from the west. On Figure 14, resistivity iso-surfaces of 10, 500 and 10000 Ohm-m are shown on top of the resistivity model extracted at a depth of 55 m. On Figure 15, chargeability iso-surfaces of 10, 20 and 40 mV/V are shown on top of the chargeability model extracted at a depth of 55 m. These 3D models are delivered in Geosoft voxel and 3Dview formats. 3D dynamic images are also supplied in PDF format.

Finally, processed data are provided in the form of Geosoft GDB databases, and raw IP data files are also delivered in ASCII DAT and Elrec BIN formats. Raw GPS data files are supplied in GDB format.

Figure 13: 3D representation of topography, viewed from west

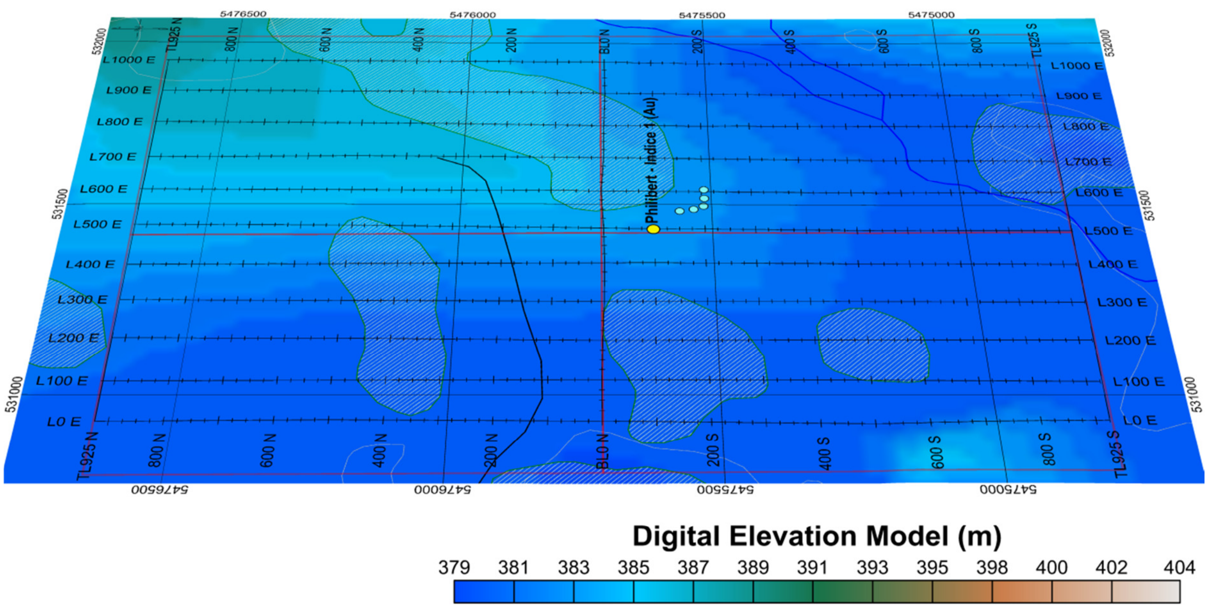

Figure 14: 3D model of resistivity distribution, viewed from west

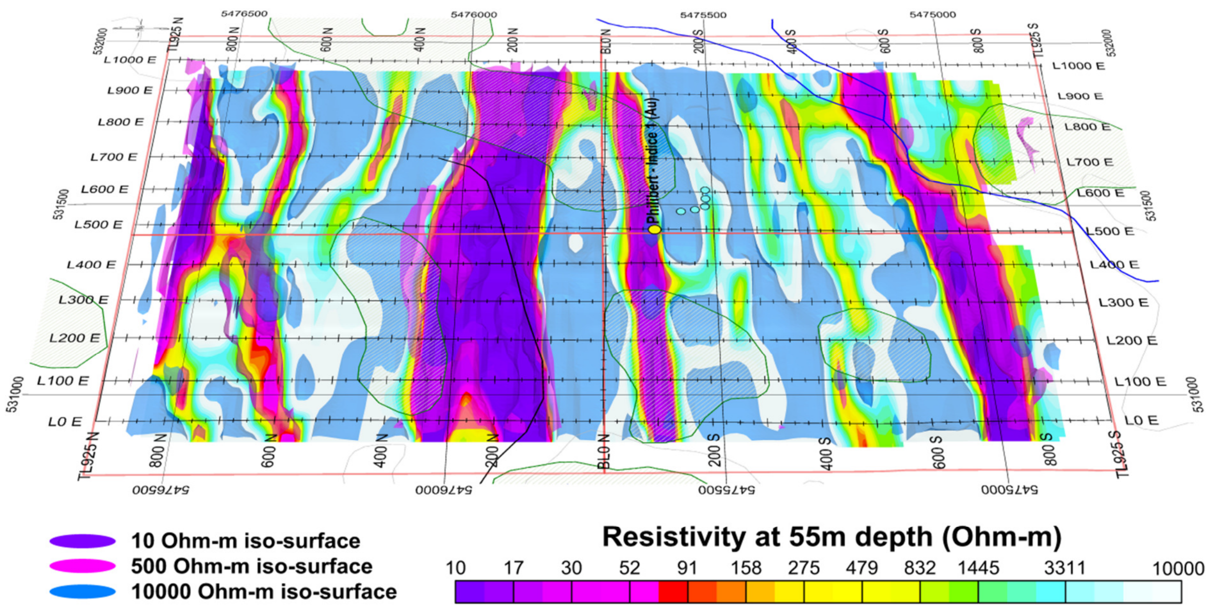

Figure 15: 3D model of chargeability distribution, viewed from west

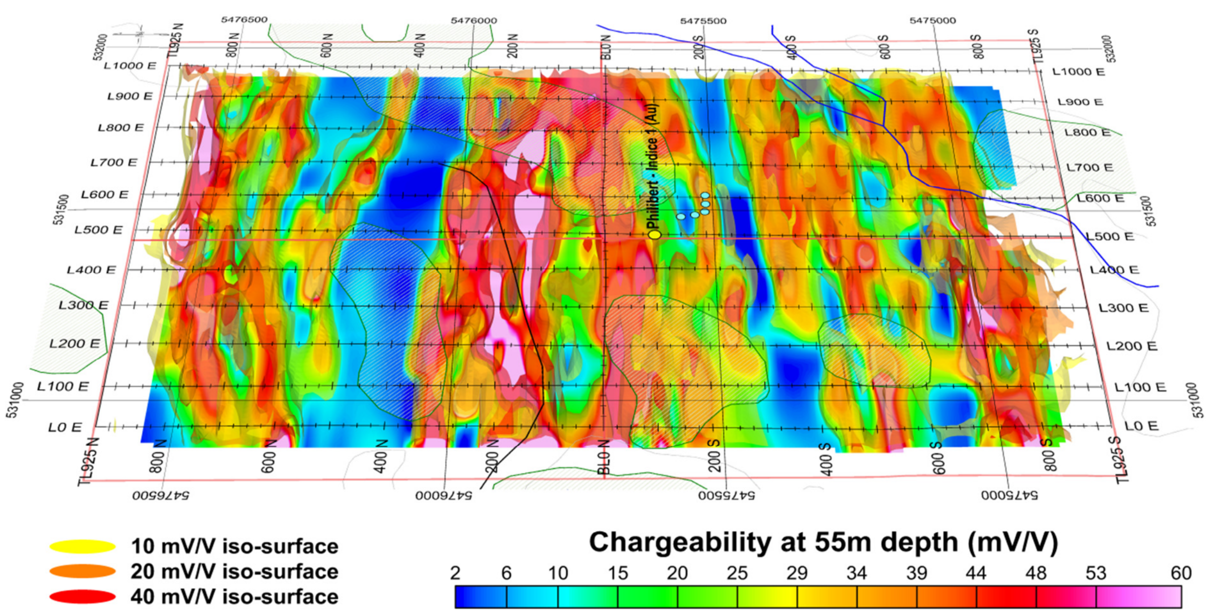

Interpretation

Table 3 summarizes relevant statistics regarding the geophysical survey performed over the Property. Strong variations are seen both for resistivity and chargeability, which denotes that the bedrock was properly investigated with the chosen electrode array.

Table 3: Statistics of recorded values for the geophysical survey

Statistic	Apparent resistivity (Ohm-m)	Apparent chargeability (mV/V)
Minimum	0.0	-8.1
5° percentile	0.2	2.7
Median	1172	23.9
Mean	2290	27.8
95° percentile	8244	66.3
Maximum	26429	386.9
Standard Deviation	3047	23.5

A strict analysis of the IP data enabled the identification of 200 chargeability anomalies among which 47 were classified as marginal, 34 as weak, 54 as moderate and 65 as strong. Location of anomaly limits along survey lines with respect to NAD-83 UTM18N coordinates, their intensity and their relation to one of the chargeable axis defined are detailed in a separate Excel spreadsheet (Ano_CHA_Philibert.xlsx) delivered with the digital PDF version of the report. It must be kept in mind that the IP method investigates a rather large 3D volume of rocks, and so anomalies found along a line could actually originate from a source offset to the side. This is usually not a problem for anomalies that are continuous over several survey lines. Significant resistivity contrasts were also identified in the vicinity of chargeable anomalies. In total, 127 resistivity contrast anomalies are reported: 111 as conductive and 16 as resistive. For each of them, details regarding their location and nature can be found in another separate Excel spreadsheet (Ano_RES_Philibert.xlsx).

Chargeability anomalies that were grouped together as chargeable axes (Figure 16 to 19) have been assigned ID names starting with the letter 'P' (for Polarizable) and ending with a number. Characteristics for each of these chargeable axes are detailed in Table 4. Notably, this table provides information about the axis' chargeability intensity, its approximate strike length, its association to a resistivity contrast, its association to a magnetic signature, the line or lines were it appears stronger, and general comments about its characteristics and the possible nature of its source. A priority order is also supplied, based on the likelihood of the anomaly axis to denote presence of mineralization of interest (1 is prioritized over 2 and so on). In total, 47 chargeable axes are listed, out of which 11 are ranked as number 1 priority, 10 as number 2, 15 as number 3 and 11 as number 4. Details from this table are also supplied in a separate Excel files (IP-Axes_Philibert.xlsx).

Lineaments seen in the chargeability, resistivity and magnetic data are mainly striking from E-W to ENE-WSW. These lineaments are indicative of the dominant orientation of rock formations found in the area. The strongest magnetic lineaments are likely related to mafic intrusive/volcanic rocks, while areas with depressed magnetic background values are probably associated to meta-sedimentary rocks.

In some areas, it is possible to detect structural features offsetting observed lineaments and causing abrupt interruption or changes of the geophysical responses. These features are typically caused by faults, fractures and shear zones. Interpretation of these structures has been carried out based on the airborne magnetics (Paul, 2014) and the newly acquired IP data. Such interpreted structures are shown as black 'S' shaped dashed lines on the interpretation map. On the Philibert area, possible brittle structures are preferentially aligned from NNE-SSW to N-S. It is noteworthy that the MERN has also interpreted E-W shear zones near some of the main E-W magnetic anomalies, and almost coincident with the strong conductors identified with this new survey. Since these possible E-W structures are considered coincident with the strongest conductors found near strong E-W magnetic anomalies, they are not marked on the figures and map to avoid overloading them with overlapping symbols. Intersections of these interpreted NNE-SSE/N-S structures with the E-W ones are considered of interest as many gold occurrences in the Chibougamau-Chapais mining camp, and in the Abitibi Sub-Province in general, are located near such intersections. Therefore, areas where chargeable axes are cross-cut by inferred structures should be paid particular attention.

The resistivity is sometimes affected by shallow conductive sediments, and this makes its interpretation more difficult. Since overburden is usually not chargeable and more conductive than the bedrock, areas with thicker overburden will appear as zones with low resistivity associated to low chargeability. Overburden thickness can thus be estimated in a relative sense by looking for this pattern on the shallow model's slices (Figures 7 and 10). Based on these principles, it appears that conductive overburden exists to some extent (for instance the resistivity 10 m depth slice is partly aligned along the dominant NNE-SSW glacial direction, and not exclusively controlled by the dominant E-W geological strike of the bedrock), but it is considered relatively thin throughout the surveyed area. Areas where both the chargeability and resistivity are increasing locally are likely to denote bedrock ridges underneath thinner overburden.

This being said, the chargeability values are mostly controlled by the amount of metallic minerals contained in the ground, including graphite, sulphides and some oxides such as magnetite, no matter if they are found as disseminated or in more massive form. Chargeability is therefore considered as the main targeting tool, and chargeability increases that are associated to resistivity decreases are likely to be caused by massive/semi-massive/stringer mineralization. However, in the exploration context of the Philibert project, strongly chargeable and conductive lineaments extending over long distances are deemed typical of formational graphitic horizons, which are known to occur in the area. The chargeable axes P-6, P-7, P-24, P-25, P-30, P-31, P-32, P-33, P-40, P-41 and P-44 could pertain to this type of features. These features could present some interest as gold can sometimes be associated with them, but most of the time they are devoided of significant mineralization.

Interpretation of the chargeability data can also be complicated by effects of no interest. For instance, a rock formation that is slightly enriched in disseminated sulphides or magnetite, and that comes closer to surface underneath overburden (which is not chargeable) will cause a chargeability anomaly. This type of anomaly related to bedrock uplift is characterized by a distinct chargeability anomaly (usually weak) associated to an increase in resistivity, which usually helps discriminating it from anomalies of interest. However, some specific mineralization types can also generate a chargeability and resistivity high response. It is for instance the case with weakly mineralized (sulphides) silicified structures, which are often of interest in gold exploration in general, and in the Philibert context in particular, as explained below.

An empirical approach can also be undertaken to try to outline areas prospective for gold on the Philibert Property. This approach consists in analysing the geological characteristics and the geophysical responses observed for the "Philibert – Indice 1" gold showing. According to MERN databases, this showing is characterized by outcropping quartz veins with some minor amounts of pyrite found in association with the gold mineralization. The veins are occurring within an E-W striking shear zone and are hosted by amphibolite rocks derived from basalt/gabbro. One vein graded 31.06 g/t Au over 1.22 m in channel sampling (Thériault, 1984). The mineralization was also confirmed in one of the five drill holes performed to test the outcrop area at some depth and returned 18.86 g/t over 0.60 m. Here it is important to note that the holes locations reported by the MERN are clearly wrong. They are rather located to the west and south of the outcropping showing, as can be seen on the maps from the work reported by Thériault. Unfortunately the actual holes can't be located accurately since the collars' coordinates are not reported and the maps are not properly georeferenced. A few conclusions can be drawn from the observations of the geophysical response in the vicinity of the "Philibert – Indice 1" showing.

- It occurs in association with a strong magnetic anomaly, near it's northern edge. This magnetic anomaly is interpreted as the signature of the basalt/gabbro related amphibolite. However, this does not necessarily imply that gold mineralization is always found in association with magnetic anomalies in the area.

- It is associated with a weakly chargeable and resistive anomaly. This is the type of IP response expected from quartz veins (which causes the resistivity increase) mineralized with only minor amounts of disseminated sulphides (which causes the weak chargeability anomaly). Based on this observation, all chargeability anomalies that are not associated with conductive responses have the potential to relate to such type of mineralized structures.

- It occurs immediately to the south of a major E-W conductor interpreted as the expression of a regional E-W shear zone by the MERN. More importantly in the author's opinion, it also occurs near a possible NNE-SSW fault interpreted from the current survey results. Therefore chargeability anomalies located near NNE-SSW/N-S interpreted faults, or near intersections of these interpreted faults with E-W conductors, are deemed of interest.

These considerations have been reflected in the priority classes detailed in Table 4 and have led to the prioritization of chargeable axes P-8, P-9, P-12, P-20, P-21, P-22, P-23, P-26, P-37, P-43 and P-45.

Table 4: Interpreted polarizable axis

Axis	Priority	Length (m)	Resistivity	Chargeability	Magnetic association	Best lines	Comments
P-1	4	100	No contrast	Marginal	Near strong high	L1000E	Marginal non-conductive mineralisation, rock formation with disseminated sulphides/graphite, bedrock uplift? Possible continuity of P-2 axis. Open to E.
P-2	4	100	No contrast	Marginal	Near strong high	L700E	Marginal non-conductive mineralisation, rock formation with disseminated sulphides/graphite, bedrock uplift? Possible continuity of P-1 axis. End of line anomaly, not well defined.
P-3	2	700	Conductive locally	Marginal to moderate	Weak high locally	L400E, L700E	Moderately chargeable and locally conductive mineralisation (disseminated sulphides/graphite). Possible continuity of P-4 axis. Open to E.
P-4	4	100	No contrast	Marginal	None	L200E	Marginal non-conductive mineralisation, rock formation with disseminated sulphides/graphite, bedrock uplift? Possible continuity of P-3 axis. End of line anomaly, not well defined.
P-5	4	-	No contrast	Marginal	None	L0E	Marginal non-conductive mineralisation, rock formation with disseminated sulphides/graphite, bedrock uplift? Possibly associated to P-6 axis. Open to W.
P-6	2	1000	Mostly conductive	Marginal to strong	Moderate high locally	L900E	Strongly chargeable and locally very conductive mineralisation (typical of graphitic conductors). Better potential for mineralization of interest in eastern part. Possibly associated to P-5 and P-7 axes. Open to both W and E.
P-7	3	1000	Very conductive	Weak to strong	Moderate high locally	L900E	Strongly chargeable and locally very conductive mineralisation (typical of graphitic conductors). Better potential for mineralization of interest in eastern part. Possibly associated to P-6 axis. Open to both W and E.
P-8	1	300	Resistive locally	Marginal to weak	Moderate high locally	L300E, L500E	Weakly chargeable non-conductive mineralisation (sulphides/graphite). Possibly associated to P-9 axis.
P-9	1	300	No contrast	Weak to moderate	None	L500E, L600E	Moderatly chargeable non-conductive mineralisation (sulphides/graphite). Possibly associated to P-8 axis.
P-10	2	700	Conductive	Weak to strong	None	L900E, L1000E	Strongly chargeable and conductive mineralisation (sulphides/graphite). Possible continuity of P-11 or P-12 axes. Open to E.
P-11	3	100	Resistive locally	Marginal	None	L200E	Marginal non-conductive mineralisation, rock formation with disseminated sulphides/graphite, bedrock uplift? Possible continuity of P-10 axis. Possibly associated to P-12 axis.
P-12	1	100	No contrast	Marginal to moderate	Moderate high	L0E, L100E	Moderatly chargeable non-conductive mineralisation (sulphides/graphite). Possibly associated to P-11 axis. Open to W.
P-13	2	200	Conductive	Weak to moderate	Strong high	L0E, L100E	Moderatly chargeable and conductive mineralisation (sulphides/graphite). Possible continuity of P-10 or P-14 axes. Open to W.
P-14	3	-	Resistive	Marginal	None	L300E	Marginal non-conductive mineralisation, rock formation with disseminated sulphides/graphite, bedrock uplift? Possible continuity of P-13 and P-15 axes.

Axis	Priority	Length (m)	Resistivity	Chargeability	Magnetic association	Best lines	Comments
P-15	2	600	Mostly conductive	Marginal to moderate	Stronghigh locally	L800E, L1000E	Moderatly chargeable and conductive mineralisation (sulphides/graphite). Possible continuity of P-14 axis. Open to E.
P-16	3	-	Resistive	Marginal	None	L1000E	Marginal non-conductive mineralisation, rock formation with disseminated sulphides/graphite, bedrock uplift? Open to E.
P-17	3	400	Resistive locally	Marginal	Near strong high locally	L0E, L200E	Marginal non-conductive mineralisation, rock formation with disseminated sulphides/graphite, bedrock uplift? Possibly associated to P-18 axis. Open to W.
P-18	2	100	Conductive locally	Moderate	Near strong high	L300E, L400E	Moderatly chargeable and conductive mineralisation (sulphides/graphite). Possibly associated to P-17 axis. Possible continuity of P-19 axis.
P-19	2	300	Conductive locally	Weak to moderate	Near strong high	L500E, L600E	Moderatly chargeable and conductive mineralisation (sulphides/graphite). Possibly associated to P-20 axis. Possible continuity of P-18 axis.
P-20	1	200	Resistive	Marginal to weak	Near strong high	L800E, L1000E	Weakly chargeable non-conductive mineralisation (sulphides/graphite). Possibly associated to P-19 and P-21 axes. Possible continuity of P-22 axis. Open to E.
P-21	1	100	Resistive and conductive locally	Moderate	Strong high	L1000E	Weakly chargeable and locally non-conductive mineralisation (sulphides/graphite). Possibly associated to P-20 and P-25 axes. Open to E.
P-22	1	100	Resistive	Marginal to weak	Strong high	L500E	Weakly chargeable non-conductive mineralisation (sulphides/graphite). Associated to the Philibert - Indice 1 showing. Possibly associated to P-24 axis. Possible continuity of P-20 and P-23 axes.
P-23	1	400	No contrast	Marginal to weak	Strong high	L200E, L400E	Weakly chargeable non-conductive mineralisation (sulphides/graphite). Possible continuity of P-22 axis. Open to W.
P-24	3	700	Very conductive	Marginal to strong	None	L100E, L300E	Strongly chargeable and locally very conductive mineralisation (typical of graphitic conductors). Possibly associated to P-22 axis. Open to W.
P-25	3	100	Very conductive	Strong	None	L1000E	Strongly chargeable and locally very conductive mineralisation (typical of graphitic conductors). Possibly associated to P-21 and P-26 axes. Open to E.
P-26	1	1000	Conductive locally	Moderate to strong	Weak high locally	L100E, L500E, L800E, L900E	Moderatly chargeable and mostly non-conductive mineralisation (sulphides/graphite). Possibly associated to P-24, P-25, P-27 and P-28 axes. Open to both W and E.
P-27	4	-	None	Marginal	None	L200E	Marginal non-conductive mineralisation, rock formation with disseminated sulphides/graphite, bedrock uplift? Possibly associated to P-26 axis.
P-28	4	-	None	Marginal	None	L500E	Marginal non-conductive mineralisation, rock formation with disseminated sulphides/graphite, bedrock uplift? Possibly associated to P-26 axis.
P-29	4	-	None	Marginal	Near strong high	L300E	Marginal non-conductive mineralisation, rock formation with disseminated sulphides/graphite, bedrock uplift? Possibly associated to P-30 axis.
P-30	3	1000	Very conductive	Strong	Strong high	L500E, L600E, L700E, L800E	Strongly chargeable and very conductive mineralisation (typical of graphitic conductors). Possibly associated to P-29, P-31 and P-32 axes. Open to both W and E.
P-31	3	400	Very conductive	Marginal to strong	Strong high	L0E, L300E	Strongly chargeable and very conductive mineralisation (typical of graphitic conductors). Possibly associated to P-30 and P-33 axes. Open to W.

Axis	Priority	Length (m)	Resistivity	Chargeability	Magnetic association	Best lines	Comments
P-32	3	100	Conductive locally	Marginal to strong	Near moderate high	L900E	Strongly chargeable and locally very conductive mineralisation (typical of graphitic conductors). Possibly associated to P-30 and P-33 axes. Open to E.
P-33	3	1000	Very conductive	Weak to strong	Moderate high mostly	L0E, L200E, L700E	Strongly chargeable and very conductive mineralisation (typical of graphitic conductors). Possibly associated to P-29, P-31 and P-32 axes. Open to both W and E.
P-34	4	-	None	Marginal	None	L1000E	Marginal non-conductive mineralisation, rock formation with disseminated sulphides/graphite, bedrock uplift? Open to E.
P-35	2	300	Mostly conductive	Weak to strong	Weak high	L700E	Strongly chargeable and locally conductive mineralisation (sulphides/graphite). Possible continuity of P-38 axis. Open to E.
P-36	3	200	Mostly resistive	Marginal	Marginal high	L400E	Marginal non-conductive mineralisation, rock formation with disseminated sulphides/graphite, bedrock uplift?
P-37	1	300	Resistive locally	Marginal to weak	None	L300E, L400E	Weakly chargeable non-conductive mineralisation (sulphides/graphite). Possible continuity of P-37 axis.
P-38	2	100	Conductive locally	Moderate to strong	Marginal high locally	L600E	Strongly chargeable and locally conductive mineralisation (sulphides/graphite). Possible continuity of P-35 and P-37 axes.
P-39	4	-	None	Marginal	None	L1000E	Marginal non-conductive mineralisation, rock formation with disseminated sulphides/graphite, bedrock uplift? Open to E.
P-40	3	800	Very conductive	Weak to strong	Weak high	L800E	Strongly chargeable and very conductive mineralisation (typical of graphitic conductors). Possibly associated to P-41 and P-43 axes. Open to E.
P-41	3	400	Very conductive	Moderate to strong	Strong high	L0E, L100E	Strongly chargeable and very conductive mineralisation (typical of graphitic conductors). Possibly associated to P-40 and P-45 axes. Possible continuity of P-42 or P-44 axes. Open to W.
P-42	4	100	No contrast	Marginal	Near strong high	L600E	Marginal non-conductive mineralisation, rock formation with disseminated sulphides/graphite, bedrock uplift? Possibly associated to P-44 axis. Possible continuity of P-41, P-43 or P-45 axes.
P-43	1	200	No contrast	Marginal to moderate	None	L900E	Moderatly chargeable non-conductive mineralisation (sulphides/graphite). Possibly associated to P-40 axis. Possible continuity of P-42 axis. Open to E.
P-44	3	500	Very conductive	Strong	Strong high	L600E, L700E, L800E	Strongly chargeable and very conductive mineralisation (typical of graphitic conductors). Possibly associated to P-42 axis. Possible continuity of P-41, P-45 or P-46 axes. Open to E.
P-45	1	300	Resistive locally	Marginal to strong	None	L400E	Strongly chargeable non-conductive mineralisation (sulphides/graphite). Possibly associated to P-41 and P-46 axes. Possible continuity of P-42 or P-44 axes.
P-46	2	400	Conductive	Marginal to moderate	Moderate high locally	L0E, L1E	Moderately chargeable and conductive mineralisation (sulphides/graphite). Possibly associated to P-45 axis. Possible continuity of P-44 axis. Open to W.
P-47	4	-	Conductive	Marginal	Near weak high	L200E	Marginally chargeable and conductive mineralisation (sulphides/graphite). End of line anomaly, not well defined.

Figure 16: Resistivity and induced polarization interpretation over DEM data

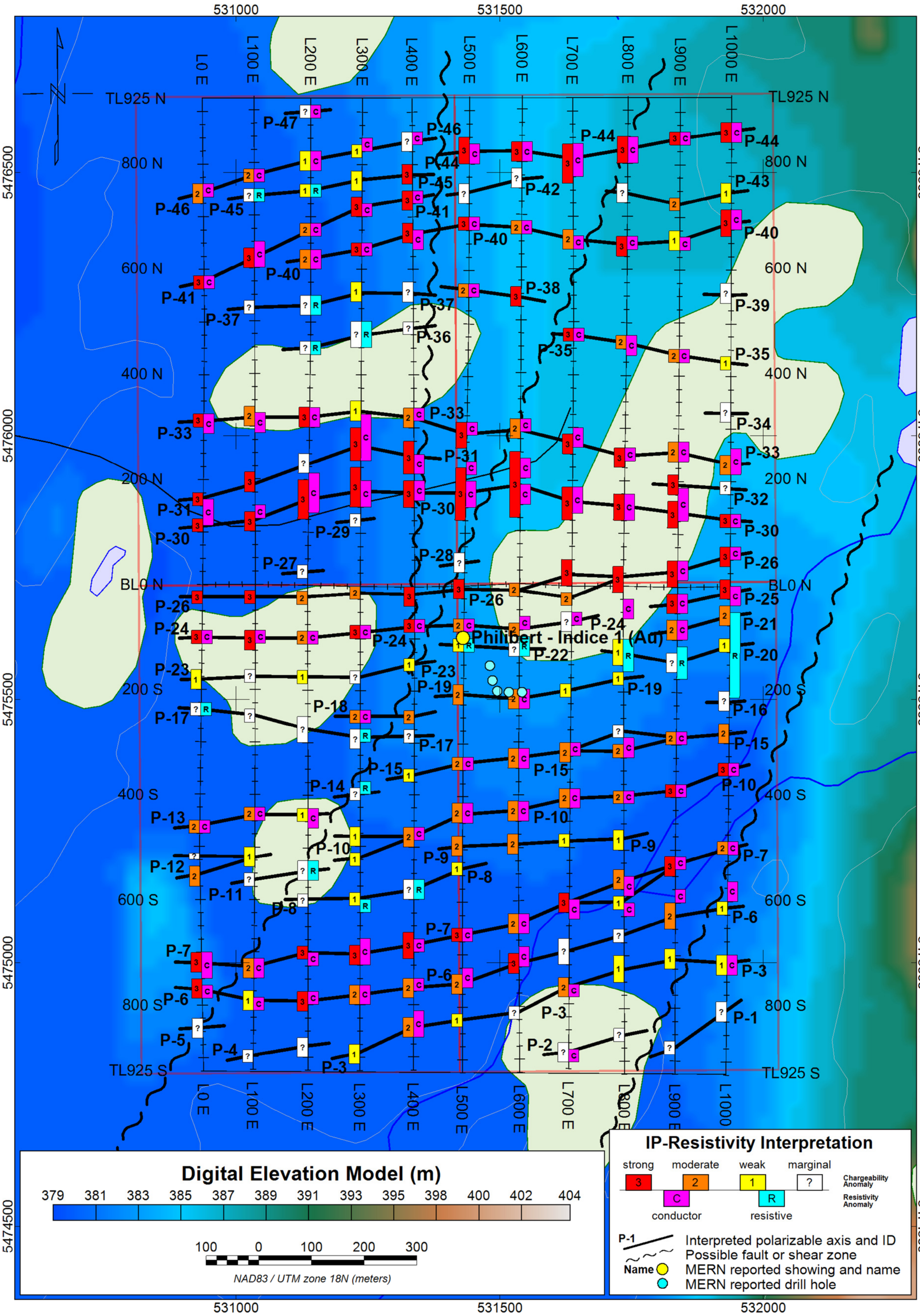

Figure 17: Resistivity and induced polarization interpretation over FVD data

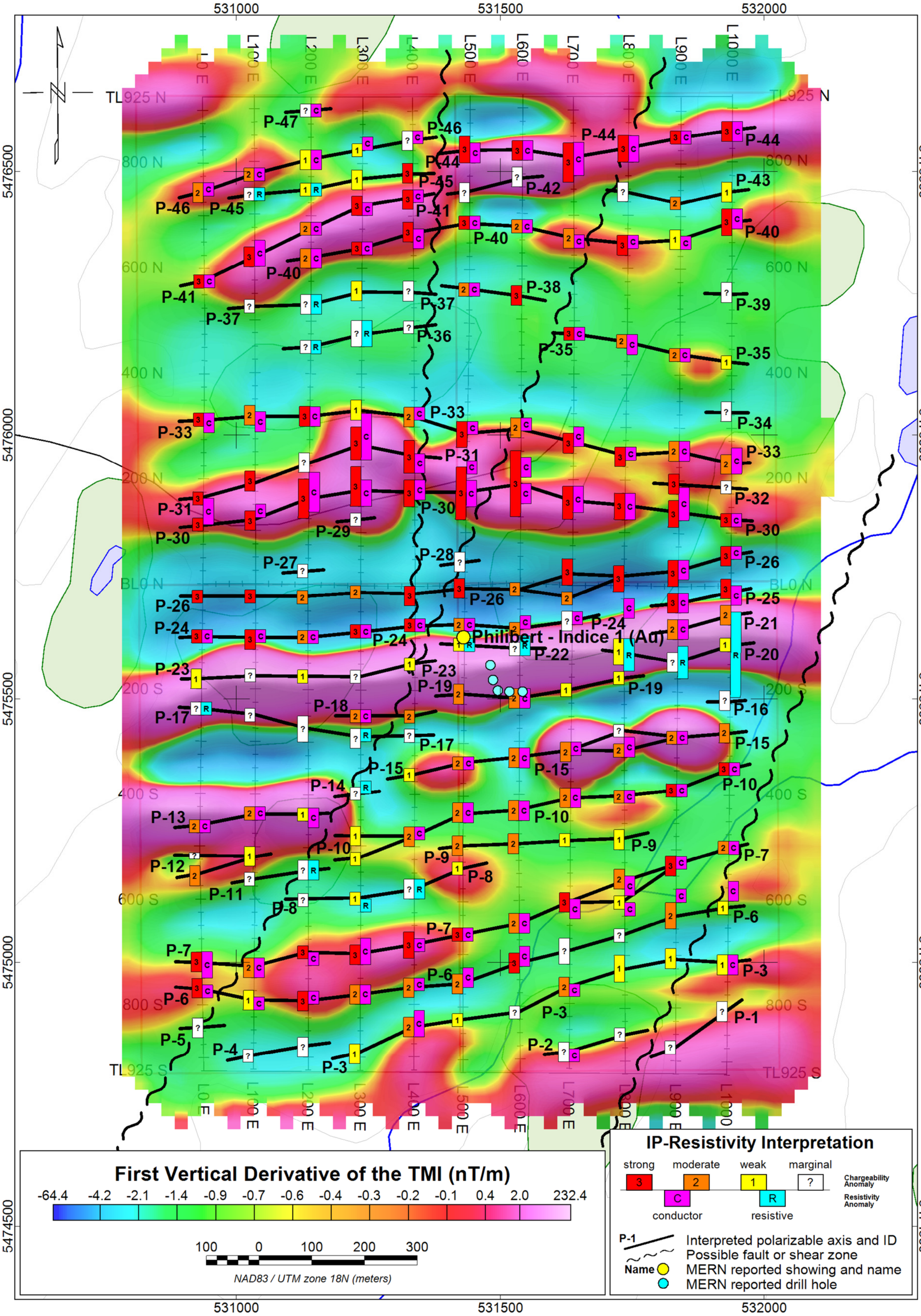

Figure 18: Resistivity and induced polarization interpretation over resistivity at 25m

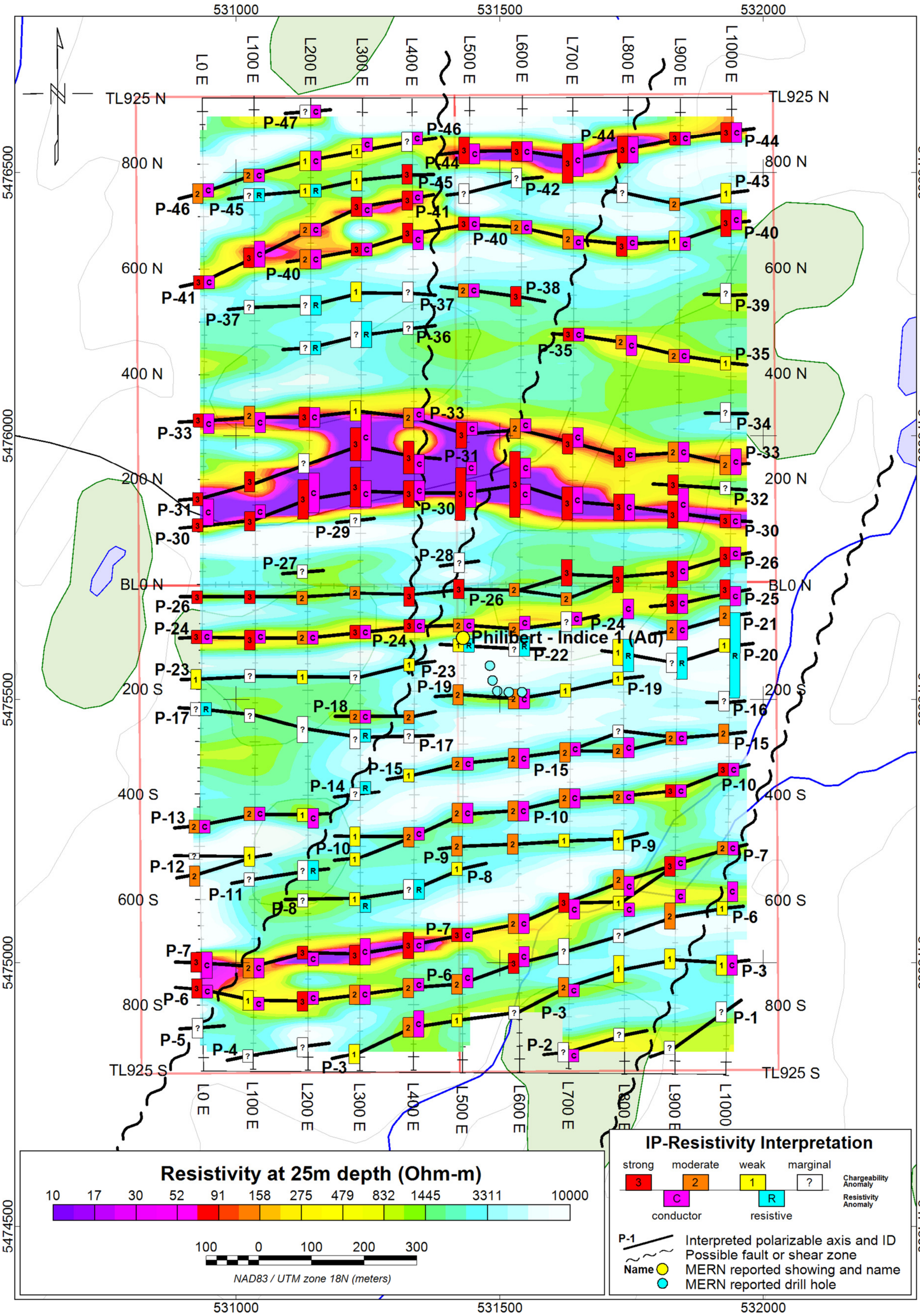

Figure 19: Resistivity and induced polarization interpretation over chargeability at 25m

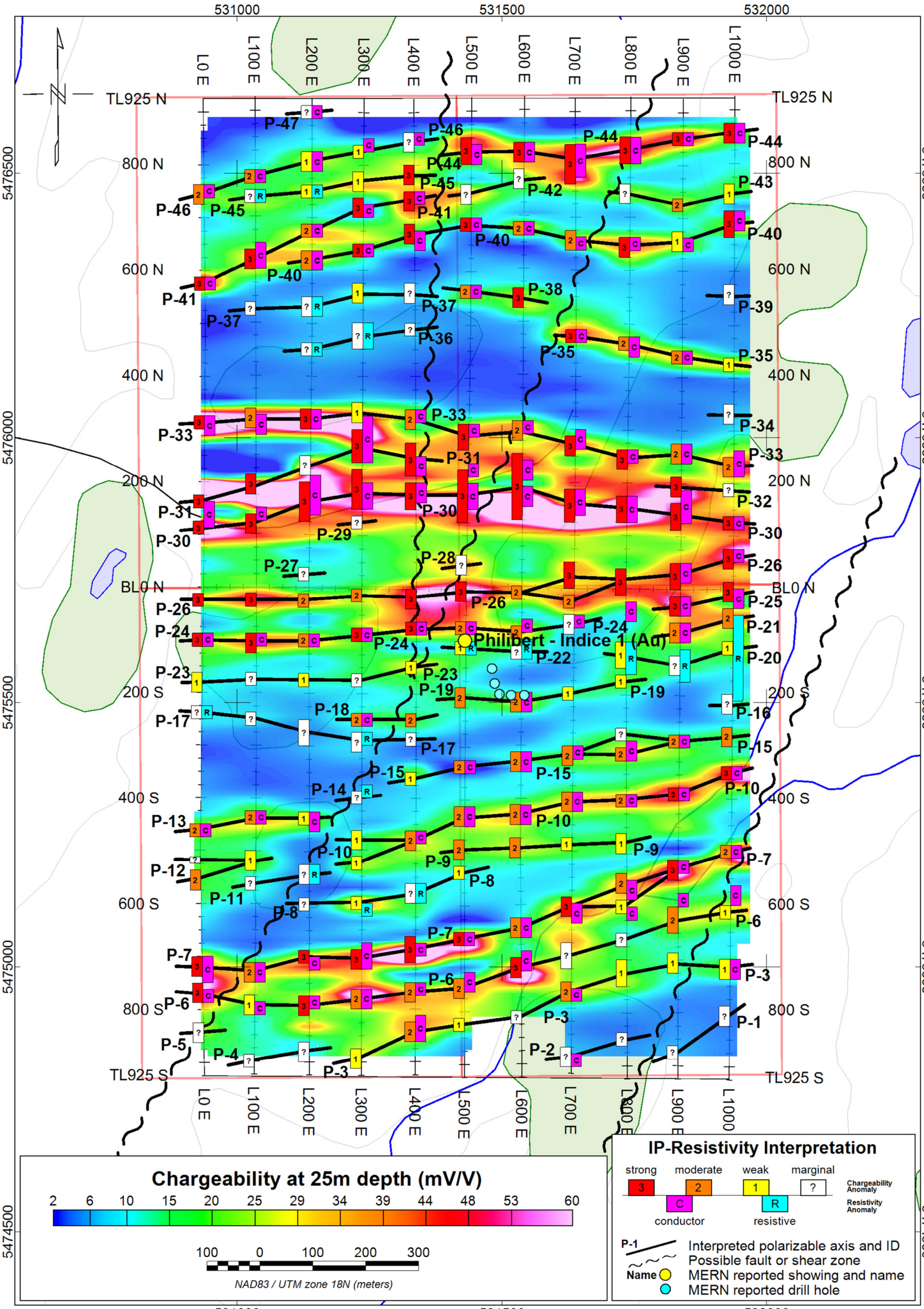

Recommendations

First of all, it is recommended to verify geological and geochemical data available in the vicinity of all priority 1 and 2 polarizable lineaments. It is recommended to investigate the outlined anomalies by basic prospection methods at first, using the provided interpretation map and table as a guide in support of this reconnaissance effort. The implementation of a geochemical soil sampling program or of a till sampling program could also help further prioritize outlined anomalies.

If interesting results are obtained, or if overburden proves too thick for prospecting, it is recommended to perform short drill holes to verify the nature of some of the selected targets. The interpretation map and IP inversion models can be used to accurately define drilling targets. The 3D model results can also be sliced in sections and used to visualize each drill target based on the geophysical data. It must be kept in mind that it is possible that mineralization of interest yields weaker responses than a source of no interest such as a sterile sulphide occurrence.

It is also recommended to compile rock sample analysis and logs eventually obtained in trenches and drill holes, considering their actual location in space. Analysis of these results in 3D in conjunction with the geophysical 3D models would possibly help better characterising the response of mineralized occurrences. Based on this, areas with similar responses would then be highly prioritized.

V. CONCLUSION

The IP survey that was conducted on the Philibert Property in November of 2018 was successful in meeting the survey objectives. Physical properties distribution were better characterised within the area, which could support a better understanding of the geological setting. The geophysical response of the gold mineralization found within the property was also better characterised, helping with the selection of exploration targets to prioritize. A total of 200 individual IP anomalies, further grouped as 47 chargeable lineaments, have been defined. Among them, 11 axes are considered with higher potential to relate to mineralized occurrences.

A basic surface prospection campaign is recommended at first for the investigation of anomalies' sources, with a concomitant geochemical soil sampling or till sampling program, to help selecting the very best geophysical anomalies for drilling follow-up. The anomaly tables listing several characteristics for each anomaly have been provided to support this exploration effort. Further compilation of available geoscience data is encouraged and would help refining the interpretation of the geophysical data.

Respectfully submitted,

____

Joël Dubé, P.Eng.
December 12th 2018

VII. REFERENCES

Thériault, G., 1984. *Rapport de la campagne d'exploration 1983-1984, Projet Philibert (100981)*; Report by SOQUEM. (Québec MERN Sigeom reference GM41259)

Paul, R. et Létourneau, O., 2014. *Rapport d'acquisition, Projet Opawica, Levé Géophysique magnétique et VLF héliporté, Région de Chibougamau, Québec*; Report by Géophysique GPR International Inc. for Stellar Africagold (Québec MERN Sigeom reference GM68155)

VIII. Statement of Qualifications

Joël Dubé
7977 Décarie Drive
Ottawa, ON, Canada, K1C 3K3

Telephone: 819.598.8486
E-mail: jdube@ddgeoscience.ca

I, Joël Dubé, P.Eng., do hereby certify that:

1. I am a consultant in geophysics, President of Dynamic Discovery Geoscience Ltd, registered in Canada.

2. I earned a Bachelor of Engineering in Geological Engineering in 1999 from the École Polytechnique de Montréal.

3. I am an Engineer registered with the Ordre des Ingénieurs du Québec, No. 122937, and a Professional Engineer with Professional Engineers Ontario, No. 100194954 (CofA No. 100219617) and with the Association of Professional Engineers and Geoscientists of New Brunswick, No. L5202 (CofA No. F1853).

4. I have practised my profession for 17 years in exploration geophysics.

5. I have not received and do not expect to receive a direct or indirect interest in the properties covered by this report.

Dated this 12th of December, 2018

____
Joël Dubé, P.Eng. #122937